forum acusticum 2026
8-12 September · Graz, Austria

# TOWARDS A LOCALISED POD-GALERKIN REDUCED-ORDER MODELLING APPROACH FOR TIME-VARYING STRUCTURAL DYNAMICS

Shing-Cheung To[1], Giacomo Squicciarini[1], Sjoerd van Ophem[1]

[1] *Institute of Sound and Vibration Research, University of Southampton, Southampton, UK*

This paper is a revised version of the authors' submitted manuscript that was peer-reviewed by at least two anonymous reviewers.



## Abstract

Parametric reduced-order models (ROMs) for linear structural dynamics commonly focus on time-invariant parametric settings. However, when parameters vary in time, the governing operators become time-dependent and ROM accuracy must be ensured over a family of admissible parameter trajectories rather than a bounded parameter domain. Direct sampling of this trajectory space is computationally prohibitive, and approximating the solution manifold using a single global basis often leads to an impractically high-dimensional reduced subspace. We therefore adopt a regime-based ROM library approach, where each local ROM is constructed by computing a proper orthogonal decomposition (POD) basis from full-order snapshots at selected constant parameter values and applying a Galerkin projection onto the resulting reduced subspace. The parameter values are chosen using a low-cost library refinement indicator based on discrepancies between adjacent local ROMs. In the online phase, the model selects the appropriate local ROM according to the active parameter regime and a mass-orthogonal projection transfers the reduced states across subspaces at regime transitions. The method is demonstrated on a Kirchhoff-Love plate with a time-varying boundary stiffness parameter, which induces a time-dependent stiffness matrix affinely. Results show that this method can achieve sufficient accuracy with substantially smaller reduced dimensions than a single global ROM.

**Keywords:** *projection-based model order reduction, finite element method, time-varying parameters, proper orthogonal decomposition*

***Corresponding author**: sct1g21@soton.ac.uk.*



## 1. Introduction

The construction of reduced-order models (ROMs) using proper orthogonal decomposition (POD) [1] is widely used to approximate large-scale dynamical systems with parametric dependence [2]. The accuracy of such models depends on the information captured in the offline full-order snapshots (i.e., the full-order degrees of freedom state vector at selected time instances) [3]. In the parametric setting, the snapshots must sufficiently cover the parameter-induced variability in the solution space. However, when parameters vary in time, snapshot generation becomes significantly more challenging, as it would, in principle, require full-order simulations of many admissible parameter trajectories so that the training data spans not only the parameter domain but also the range of possible trajectory shapes. This quickly becomes computationally prohibitive. Moreover, because the system response now depends on the entire parameter trajectory rather than a fixed parameter value, the solution manifold becomes significantly larger. Consequently, maintaining accuracy over this parameter space using a single global basis typically requires an impractically large dimensional reduced subspace.

A common approach for addressing the limitations associated with a high-dimensional global basis is to introduce an adaptive reduced subspace. In this paper, we realise this approach by employing a library of local ROMs [4] constructed from a POD-Galerkin method. Crucially, rather than sampling the space of time-varying parameter trajectories, the offline stage trains ROMs only at a set of carefully selected constant parameter values. An adaptive algorithm is proposed to identify these values and build the ROM library efficiently.

We demonstrate the approach on a Kirchhoff-Love plate excited by a point load, with time-variation introduced only through an affine boundary-spring stiffness. Extensions to multi-parameter variation are left for future work.

The remainder of this paper is organised as follows.

Section 2 introduces the full-order finite element model of the Kirchhoff-Love plate with time-varying boundary stiffness. Section 3 presents the local reduced-order modelling approach, while Section 4 details the construction of a single global ROM used for baseline comparison. Section 5 reports the numerical results. Finally, Section 6 concludes the paper and outlines directions for future work.

## 2. Numerical model

Consider an isotropic, homogeneous Kirchhoff-Love plate occupying the mid-surface domain $\Omega \subset \mathbb{R}^2$ with boundary $\Gamma$. The transverse displacement $w(x, y, t)$ satisfies:

$$D\,\nabla^4 w + \rho h\, w_{tt} = q(x, y, t), \qquad \text{in } \Omega, \tag{1}$$

where $D = \frac{Eh^3}{12(1-v^2)}$ is the bending stiffness (with Young's modulus $E$, Poisson's ratio $v$ and thickness $h$), $\rho$ is the material density, and $q(x, y, t)$ is the transverse load per unit area; $\nabla^4$ is the biharmonic operator. A uniformly distributed spring stiffness $k(t)$ acts along the boundary, and is introduced variationally through the boundary term $\int_\Gamma k(t) w v \mathbf{d}s$, where $v$ is an admissible test function. Eq. (1) is discretised by a standard Galerkin finite element method (FEM) using $C^1$ conforming Bogner-Fox-Schmit bicubic rectangular elements with nodal degrees of freedom (DOFs) $[w, w_x, w_y, w_{xy}]$. This yields the semi-discrete full-order system

$$\mathbf{M}\ddot{\mathbf{d}}(t) + \mathbf{C}\dot{\mathbf{d}}(t) + \mathbf{K}(t)\mathbf{d}(t) = \mathbf{B}\mathbf{u}(t), \tag{2}$$

$$\mathbf{y}(t) = \mathbf{L}\mathbf{d}(t), \tag{3}$$

where $\mathbf{d}(t) \in \mathbb{R}^n$ is the global DOF vector, with $n$ being the number of DOFs of the finite element mesh, $\mathbf{u}(t) \in \mathbb{R}^m$ is the input signal, with $m$ being the number of inputs, $\mathbf{B} \in \mathbb{R}^{n\times m}$ is the spatial input matrix, $\mathbf{y}(t) \in \mathbb{R}^p$ is the output vector with $p$ being the number of outputs, and $\mathbf{L} \in \mathbb{R}^{p\times n}$ is the output matrix. $\mathbf{M}$, $\mathbf{C}$ and $\mathbf{K}$ are the global mass, damping and stiffness matrices, where $\mathbf{C}$ has been introduced on the semi-discrete level by assuming Rayleigh damping by taking $\mathbf{C} = \alpha_M \mathbf{M} + \beta_K \mathbf{K}_{\text{plate}}$, where $\alpha_M$ and $\beta_K$ are constants, and $\mathbf{K}_{\text{plate}}$ is the constant plate bending stiffness contribution. The global stiffness matrix $\mathbf{K}(t)$ is decomposed as

$$\mathbf{K}(t) = \mathbf{K}_{\text{plate}} + \mathbf{K}_{\text{edge}}(t), \tag{4}$$

where $\mathbf{K}_{\text{edge}}(t)$ is the time-varying boundary-spring contribution and takes the form,

$$\mathbf{K}_{\text{edge}}(t) = k(t)\mathbf{K}^0_{\text{edge}}, \tag{5}$$

where $k(t)$ is the scalar time varying boundary stiffness and $\mathbf{K}^0_{\text{edge}}$ is the unit boundary-spring stiffness matrix. Hence,

$$\mathbf{K}(t) = \mathbf{K}_{\text{plate}} + k(t)\mathbf{K}^0_{\text{edge}}. \tag{6}$$

Eqs. (2) and (3) are integrated in time using the generalised-$\alpha$ method (with parameters set by $\rho_\infty$) [5]. The time-varying stiffness matrix $\mathbf{K}(t)$ and input $\mathbf{u}(t)$ are evaluated at the generalised-$\alpha$ level using linear interpolation between successive time steps.

## 3. Method

### 3.1. Training

Local ROMs are trained on a set of chosen constant boundary stiffness values $k_i$, i.e. stiffness values that do not vary in time. The selection strategy for these stiffness values is detailed in Section 3.6. We assume that the external forcing is known a priori and remains the same across all full-order training simulations. For a given training value $k_i$, we solve the full-order model (FOM) with the time-invariant stiffness matrix

$$\mathbf{K}_i = \mathbf{K}_{\text{plate}} + \mathbf{K}_{\text{edge},i} = \mathbf{K}_{\text{plate}} + k_i \mathbf{K}^0_{\text{edge}}. \tag{7}$$

This affine form allows for efficient updates to the boundary stiffness contribution $\mathbf{K}_{\text{edge},i}$, since $\mathbf{K}^0_{\text{edge}}$ is assembled only once and subsequent evaluations of $\mathbf{K}_{\text{edge},i}$ for different $k_i$ reduce to a simple scalar-matrix multiplication.

### 3.2. Snapshot collection

The FOM is sampled uniformly with an interval of $\Delta t_s$, which must be sufficiently small so that all relevant dynamical features are well approximated in the resulting reduced local basis. Snapshots are taken from the full-order state $\mathbf{d}(t)$ at snapshot times $\{t_x\}_{x=1}^{N_s}$. The snapshot matrix $\mathbf{S}_i$ for a given $k_i$ is

$$\mathbf{S_i} = \left[\mathbf{d}_i(t_1)\ \mathbf{d}_i(t_2)\ \cdots\ \mathbf{d}_i(t_{N_s})\right] \in \mathbb{R}^{n\times N_s}. \tag{8}$$

### 3.3. POD basis

We perform a POD on Eq. (8) via the method of snapshots. For a given snapshot matrix $\mathbf{S}_i$ and mass matrix $\mathbf{M}$, we define the correlation matrix as

$$\mathbf{C}_i = \mathbf{S}_i^\top \mathbf{M} \mathbf{S}_i \in \mathbb{R}^{N_s\times N_s}. \tag{9}$$

We then solve the eigenvalue problem,

$$\mathbf{C}_i \mathbf{w}_j = \lambda_j \mathbf{w}_j, \tag{10}$$

where $\lambda_j$ and $\mathbf{w}_j \in \mathbb{R}^{N_s}$ denote the $j$-th eigenvalue and eigenvector, respectively. The POD singular values satisfy $\sigma_j = \sqrt{\lambda_j}$. A reduced basis $\mathbf{V}_i \in \mathbb{R}^{n\times r}$ is then constructed as

$$\mathbf{V}_i = \mathbf{S}_i \mathbf{W}_r \mathbf{\Lambda}_r^{-1/2}, \tag{11}$$

where $\mathbf{W}_r = [\mathbf{w}_1, \ldots, \mathbf{w}_r] \in \mathbb{R}^{N_s\times r}$ and $\mathbf{\Lambda}_r = \text{diag}(\lambda_1, \ldots, \lambda_r) \in \mathbb{R}^{r\times r}$. This construction yields a mass-orthonormal basis $\mathbf{V}_i^\top \mathbf{M} \mathbf{V}_i = \mathbf{I}$, where $\mathbf{I}$ denotes the identity matrix.

For simplicity, all local bases $\mathbf{V}_i$ are constructed with a fixed reduced dimension $r$, where the value of $r$ is chosen to provide an adequate accuracy-size trade-off, typically with POD eigenvalues $\lambda_j$ rapidly decaying beyond this truncation. Although variable local dimensions $r_i$ are possible, they are not considered here

for clarity; this extension is left for future work.

### 3.4. Coordinate alignment

When POD singular values $\sigma_j$ are equal or closely clustered, the corresponding singular vectors are not uniquely defined; any orthogonal rotation within the corresponding reduced subspace yields another valid basis. Consequently, different snapshot sets can yield bases that span very similar reduced subspaces (e.g., from nearby parameter values) but whose columns are rotated, permuted, or sign-flipped. Although this ambiguity does not change the span of the reduced subspace, it makes the reduced coordinates incompatible across different bases. To ensure consistent reduced coordinates across the bases, each basis $\mathbf{V}_i$ is rotated to align with a reference basis $\mathbf{V}_{\text{ref}}$ using a mass-inner product Procrustes rotation. In this paper, we take the reference basis as the POD basis constructed from the first training stiffness value in the offline phase.

Consider we have a reference basis $\mathbf{V}_{\text{ref}}$ and a local reduced basis $\mathbf{V}_i$. We want to find a rotation $\mathbf{R} \in \mathbb{R}^{r\times r}$ with $\mathbf{R}^\top\mathbf{R} = \mathbf{I}$ that makes $\mathbf{V}_i\mathbf{R}$ as close as possible to $\mathbf{V}_{\text{ref}}$ in the mass-weighted Frobenius norm. This yields the optimisation problem [6],

$$\arg\min_{\mathbf{R}^T\mathbf{R}=\mathbf{I}} \|\mathbf{V}_i\mathbf{R} - \mathbf{V}_{\text{ref}}\|^2_{\mathbf{M},\mathbf{F}}\,, \tag{12}$$

where the mass-weighted Frobenius norm is $\|\mathbf{A}\|_{\mathbf{M},\mathbf{F}} := \sqrt{\text{tr}(\mathbf{A}^\top\mathbf{M}\mathbf{A})}$. This is equivalent to maximising a trace term,

$$\arg\max_{\mathbf{R}^\top\mathbf{R}=\mathbf{I}} \text{tr}(\mathbf{R}^\top\mathbf{V}_i^\top\mathbf{M}\mathbf{V}_{\text{ref}}). \tag{13}$$

To solve Eq. (13), we take the singular value decomposition (SVD) of

$$\mathbf{J}_i = \mathbf{V}_i^\top\mathbf{M}\mathbf{V}_{\text{ref}}, \tag{14}$$

where $\mathbf{J}_i$ is decomposed as

$$\mathbf{J}_i = \mathbf{U}_i\mathbf{\Sigma}_i\mathbf{W}_i^\top, \tag{15}$$

where $\mathbf{U}_i$ and $\mathbf{W}_i$ are the left and right singular vectors of $\mathbf{J}_i$, respectively. The optimal rotation $\mathbf{R}_i^*$ is therefore

$$\mathbf{R}_i^* = \mathbf{U}_i\mathbf{W}_i^\top, \tag{16}$$

and the aligned basis is

$$\mathbf{V}_{\text{aligned},i} = \mathbf{V}_i\mathbf{R}_i^*. \tag{17}$$

Since $\mathbf{R}_i^*$ is orthogonal, the mass-orthonormality of the POD bases are preserved. For simplicity, in the subsequent sections we will overwrite the aligned basis and continue to denote it as $\mathbf{V}_i$.

### 3.5. Galerkin projection

For each local basis $\mathbf{V}_i$, the state is approximated as

$$\mathbf{d}(t) \approx \mathbf{V}_i\mathbf{q}_i(t), \tag{18}$$

where $\mathbf{q}_i(t) \in \mathbb{R}^r$ are the reduced coordinates. Projecting the FOM onto the reduced subspace span$(\mathbf{V}_i)$, yields the reduced system

$$\mathbf{M}_{r,i}\ddot{\mathbf{q}}_i(t) + \mathbf{C}_{r,i}\dot{\mathbf{q}}_i(t) + \mathbf{K}_{r,i}(k_i)\,\mathbf{q}_i(t) = \mathbf{B}_{r,i}\mathbf{u}(t), \tag{19}$$

$$\mathbf{y}_{r,i}(t) = \mathbf{L}_{r,i}\mathbf{q}_i(t), \tag{20}$$

where

$$\mathbf{M}_{r,i} = \mathbf{V}_i^\top\mathbf{M}\mathbf{V}_i, \tag{21}$$

$$\mathbf{C}_{r,i} = \mathbf{V}_i^\top\mathbf{C}\mathbf{V}_i, \tag{22}$$

$$\mathbf{B}_{r,i} = \mathbf{V}_i^\top\mathbf{B}, \tag{23}$$

$$\mathbf{L}_{r,i} = \mathbf{V}_i\mathbf{L}, \tag{24}$$

$$\mathbf{K}_{r,i}(k_i) = \underbrace{\mathbf{V}_i^\top\,\mathbf{K}_{\text{plate}}\,\mathbf{V}_i}_{\mathbf{K}_{\text{plate},r,i}} + k_i\,\underbrace{\mathbf{V}_i^\top\,\mathbf{K}^0_{\text{edge}}\,\mathbf{V}_i}_{\mathbf{K}^0_{\text{edge},r,i}}. \tag{25}$$

### 3.6. Local ROM library construction

We construct an adaptive library of local ROMs $\mathcal{L} = \{\text{ROM}(k_i)\}_{i=1}^{N_{\text{lib}}}$ over a prescribed stiffness interval $[k_{\min}, k_{\max}]$, where $k_{\min}$ and $k_{\max}$ denote the minimum and maximum stiffness values, respectively, and $N_{\text{lib}}$ is the number of local ROMs. Each entry in the library stores the corresponding training stiffness value $k_i$, the local basis $\mathbf{V}_i$, and the reduced operators $\mathbf{M}_{r,i}$, $\mathbf{C}_{r,i}$, $\mathbf{B}_{r,i}$, $\mathbf{L}_{r,i}$, $\mathbf{K}_{\text{plate},r,i}$, and $\mathbf{K}^0_{\text{edge},r,i}$. The objective is to obtain a compact set of training values $\{k_i\}$ that yields accurate predictions for time-varying stiffness trajectories $k(t)$ with minimal offline cost.

Consider a current interval whose endpoints correspond to two consecutive stiffness values in this set. We denote this interval by $[k_a, k_b]$, where ROM$(k_a)$ and ROM$(k_b)$ are the local ROMs trained at stiffness values $k_a$ and $k_b$, respectively. Within this interval, we select $n_{\text{probe}}$ probe stiffness values $\{k^{(p)}\}_{p=1}^{n_{\text{probe}}} \in (k_a, k_b)$ by uniform spacing in $\log_{10} k$

$$k^{(p)} = 10^{\log_{10}(k_a) + \frac{p}{n_{\text{probe}}+1}(\log_{10}(k_b) - \log_{10}(k_a))}, \tag{26}$$

where $p = 1, \ldots, n_{\text{probe}}$. These probe values are used to evaluate both endpoint ROMs at the intermediate stiffnesses by forming their corresponding reduced stiffness matrices as

$$\begin{aligned}\mathbf{K}_r^{(k_a)}(k^{(p)}) &= \mathbf{K}^{(k_a)}_{\text{plate,r}} + k^{(p)}\mathbf{K}^{0(k_a)}_{\text{edge,r}},\\ \mathbf{K}_r^{(k_b)}(k^{(p)}) &= \mathbf{K}^{(k_b)}_{\text{plate,r}} + k^{(p)}\mathbf{K}^{0(k_b)}_{\text{edge,r}},\end{aligned} \tag{27}$$

where the superscript $(k_a)$ (respectively $(k_b)$) indicates operators obtained by projection with the basis trained at $k_a$ (respectively $k_b$), e.g.

$$\mathbf{K}^{(k_a)}_{\text{plate,r}} = \mathbf{V}^T_{k_a}\mathbf{K}_{\text{plate}}\mathbf{V}_{k_a}, \mathbf{K}^{0(k_a)}_{\text{edge,r}} = \mathbf{V}^T_{k_a}\mathbf{K}^0_{\text{edge}}\mathbf{V}_{k_a}, \tag{28}$$

where $\mathbf{V}_{k_a}$ denotes the local basis trained at constant stiffness $k_a$. For each probe $k^{(p)}$, we compute the corresponding displacement output time histories $\mathbf{y}_r^{(k_a)}(k^{(p)}) \in \mathbb{R}^{N_t}$ and $\mathbf{y}_r^{(k_b)}(k^{(p)}) \in \mathbb{R}^{N_t}$ and define

the relative disagreement $\eta(k^{(p)})$,

$$\eta(k^{(p)}) = \frac{\left\| \mathbf{y}_r^{(k_a)}(k^{(p)}) - \mathbf{y}_r^{(k_b)}(k^{(p)}) \right\|_2}{\max\left( \left\| \mathbf{y}_r^{(k_a)}(k^{(p)}) \right\|_2, \left\| \mathbf{y}_r^{(k_b)}(k^{(p)}) \right\|_2 \right)}. \tag{29}$$

Let $p^*$ denote the probe index at which $\eta(k^{(p)})$ is maximised, and set $k^* = k^{(p^*)}$. If $\eta(k^*) > \eta_{\text{tol}}$, we insert $k^*$ as a new training point and split the interval into $[k_a, k^*]$ and $[k^*, k_b]$. The procedure is repeated for the new intervals and refinement stops when the disagreement tolerance $\eta_{\text{tol}}$ is satisfied. Algorithm 1 summarises the procedure.

**Algorithm 1:** ROM library refinement algorithm

**Inputs:** $[k_{\min}, k_{\max}]$, $n_{\text{probe}}$, $\eta_{\text{tol}}$
**Output:** $\mathcal{L} = \{\text{ROM}(k_i)\}_{i=1}^{N_{\text{lib}}}$

1: **Construct endpoint ROMs.**
$\text{ROM}_{k_{\min}}$ and $\text{ROM}_{k_{\max}}$.

2: **Initialise library and interval list.**
$\mathcal{L} \leftarrow \{\text{ROM}_{k_{\min}}, \text{ROM}_{k_{\max}}\}$,
$\mathcal{Q} \leftarrow \{[k_{\min}, k_{\max}]\}$.
i.e., $\mathcal{Q}$ denotes a worklist of stiffness intervals pending refinement.

3: **While** $\mathcal{Q} \neq \varnothing$:

3:1. **Remove an interval** $[k_a, k_b] \subset [k_{\min}, k_{\max}]$ **from** $\mathcal{Q}$.

3:2. **Retrieve endpoint ROMs** $\text{ROM}(k_a)$, $\text{ROM}(k_b)$ **from** $\mathcal{L}$.

3:3. **Generate probe points.** $\{k^{(p)}\}_{p=1}^{n_{\text{probe}}} \subset (k_a, k_b)$,

3:4. **Compute** $\eta(k^{(p)})$ **for all probes.**

3:5. **Let** $k^* = \arg\max_{k^{(p)}} \eta(k^{(p)})$.

3:6. **If** $\eta(k^*) < \eta_{\text{tol}}$ **continue.**

3:7. **Else: Construct ROM at** $k^*$ **and add to** $\mathcal{L}$**; split** $[k_a, k_b]$ **into** $[k_a, k^*]$, $[k^*, k_b]$ **and push into** $\mathcal{Q}$.

4: **Return local ROM library.**

### 3.7. Online-phase: local ROM switching

Once the library of ROMs $\mathcal{L} = \{\text{ROM}(k_i)\}_{i=1}^{N_{\text{lib}}}$ is constructed, the online-phase proceeds by selecting the most appropriate local ROM for the current parameter stiffness value. At each time step $t_n$, we select the active local ROM using nearest-neighbour selection:

$$i(n) = \arg\min_i |k(t_n) - k_i|. \tag{30}$$

Changes in $i(n)$ define switching indices and partition the time interval into regimes on which a local basis $\mathbf{V}_i$ remains active. On each regime, the reduced operators are fixed, but the reduced stiffness matrix is updated according to

$$\mathbf{K}_{r,i}(t_n) = \mathbf{K}_{\text{plate,r,i}} + k(t_n)\mathbf{K}^0_{\text{edge,r,i}}. \tag{31}$$

A switch occurs at time $t_{\text{switch}}$ when $i(n)$ changes from one index to another. At this switch, the reduced coordinates must be projected between bases to maintain continuity. Let $\mathbf{V}_1$ and $\mathbf{V}_2$ denote the bases before and after the switch, and let $\mathbf{q}_1(t_{\text{switch}})$ and $\mathbf{q}_2(t_{\text{switch}})$ be the reduced coordinates immediately before and after switching, respectively. We obtain the initial reduced coordinate in the new active basis $\mathbf{V}_2$ by mass-orthogonal projection of the reconstructed full-order state:

$$\mathbf{q}_2(t_{\text{switch}}) = (\mathbf{V}_2^\top \mathbf{M}\mathbf{V}_2)^{-1}\mathbf{V}_2^\top \mathbf{M}\mathbf{V}_1\, \mathbf{q}_1(t_{\text{switch}}). \tag{32}$$

Since the bases are mass-orthonormal, $(\mathbf{V}_2^\top \mathbf{M}\mathbf{V}_2)^{-1} = \mathbf{I}$, Eq. (32) simplifies to $\mathbf{q}_2(t_{\text{switch}}) = \mathbf{V}_2^\top \mathbf{M}\mathbf{V}_1\, \mathbf{q}_1(t_{\text{switch}})$. It should be noted that Eq. (32) involves products with the full-order mass matrix. In an online-efficient implementation, this cost can be moved offline by precomputing the state-transfer matrix $\mathbf{T}_{2\leftarrow 1} = (\mathbf{V}_2^\top \mathbf{M}\mathbf{V}_2)^{-1}\mathbf{V}_2^\top \mathbf{M}\mathbf{V}_1 \in \mathbf{R}^{r\times r}$. The online state transfer then reduces to $\mathbf{q}_2(t_{\text{switch}}) = \mathbf{T}_{2\leftarrow 1}\mathbf{q}_1(t_{\text{switch}})$, removing online computations that scale with the full-order dimension at the cost of additional offline computations and storage.

## 4. Single global ROM

For comparison, we additionally form a single global ROM so that its performance can be assessed against the local reduced-order modelling approach when subjected to the same time-dependent stiffness variations. We construct the single global reduced basis $\mathbf{V}_{\text{global}}$ by taking the POD of the concatenated local bases $\mathbf{A}$ that form the library of local ROMs as detailed in Section 3:

$$\mathbf{A} = [\mathbf{V}_1\ \mathbf{V}_2\ \cdots\ \mathbf{V}_{N_{\text{lib}}}] \in \mathbb{R}^{n\times(rN_{\text{lib}})}. \tag{33}$$

The POD procedure is the same used for the snapshot matrix $\mathbf{S}_i$, but with $\mathbf{A}$ in place of the snapshot matrix. The single global ROM is then formed analogously to Eqs. (19)–(25) using $\mathbf{V}_{\text{global}}$.

## 5. Results

This section evaluates the accuracy and computational characteristics of the method detailed in Section 3 against a FOM. The method is also assessed against a single global ROM construction.

### 5.1. Setup

The Kirchhoff-Love plate is modelled as an aluminium rectangular plate with properties as detailed in Table 1. The simulation parameters are detailed in Table 2. The local ROM dimension $r = 12$ and snapshot sampling interval $\Delta t_s$ are chosen to provide a practical accuracy-cost trade-off in this demonstration example.

Using these settings, the local ROM reproduces the full-order response at the training stiffness values $k_i$ to within an acceptable tolerance.

**Table 1:** Plate properties.

| Quantity | Symbol | Value |
|---|---|---|
| Plate dimensions | $a \times b$ | $1.0 \times 2.0$ m |
| Thickness | $h$ | $3.0 \times 10^{-3}$m |
| Young's Modulus | $E$ | $70 \times 10^{9}$Pa |
| Poisson's ratio | $\nu$ | 0.33 |
| Density | $\rho$ | 2700kgm$^{-3}$ |

**Table 2:** Simulation parameters.

| Quantity | Symbol | Value |
|---|---|---|
| Total DOFs | $n$ | 484 |
| Number of nodes | $N_{\text{nodes}}$ | $n/4$ |
| Stiffness range | $k_{\min}, k_{\max}$ | $10^2$ N/m$^2$ to $10^6$ N/m$^2$ |
| Rayleigh coefficients | $\alpha_M, \beta_K$ | $\alpha_M = 0.8$ $\beta_K = 2 \times 10^{-5}$ |
| Generalised-alpha parameter | $\rho_\infty$ | 0.8 |
| Start/end time | $t_{\text{start}}, t_{\text{end}}$ | $0s, 10s$ |
| Time step | $dt$ | $10^{-3}$ s |
| Sampling interval | $\Delta t_s$ | $20 \times t_n$ s |
| local ROM dimension | $r$ | 12 |
| Disagreement tolerance | $\eta_{\text{tol}}$ | 8% |
| Number of probes | $n_{\text{probe}}$ | 4 |

### 5.2. Forcing

The plate is excited by a single point load applied at the plate centre $(a/2, b/2)$, such that $\mathbf{u} = u(t) \in \mathbb{R}$ and $\mathbf{B} = \mathbf{b} \in \mathbb{R}^{n\times 1}$, where $u(t)$ is the prescribed forcing time history and $\mathbf{b}$ is the associated finite-element spatial input vector. In the results presented, $u(t)$ is taken as a band-limited impulse train constructed by low-pass filtering an impulse signal with an FIR filter with cutoff frequency at 100 Hz.

### 5.3. Adaptive library construction

The disagreement metric Eq. (29) is computed using only the transverse displacement at $(a/2, b/2)$ to keep the offline training inexpensive. Following Algorithm 1, we obtain a library of $N_{\text{lib}} = 28$ local ROMs over $[10^2, 10^6]$ N/m$^2$.

### 5.4. ROM errors

To assess the accuracy of the ROM approach, we evaluate the relative errors $E$ over the nodal transverse displacement of the plate:

$$E = \frac{\|\mathbf{W}_{\text{FOM}} - \mathbf{W}_{\text{ROM}}\|_{\mathbf{F}}}{\|\mathbf{W}_{\text{FOM}}\|_{\mathbf{F}}}, \tag{34}$$

where $\|\cdot\|_{\mathbf{F}}$ denotes the Frobenius norm. The matrix $\mathbf{W}_{\text{FOM}} \in \mathbb{R}^{N_t \times N_{\text{nodes}}}$ contains the transverse nodal displacements evaluated by the FOM, with $N_t = \frac{t_{\text{end}} - t_{\text{start}}}{dt}$ denoting the number of time samples. Similarly, $\mathbf{W}_{\text{ROM}} \in \mathbb{R}^{N_t \times N_{\text{nodes}}}$ contains the transverse nodal displacements evaluated by the ROM. All errors are evaluated over the full simulation interval $[t_{\text{start}}, t_{\text{end}}]$.

### 5.5. Simulations

Figure 1 illustrates the transverse displacement at the plate centre for a stiffness trajectory that varies linearly across the entire training interval $[k_{\min}, k_{\max}]$. For this case, the local ROM yields a relative error of $E_{\text{local}} = 0.0086$ using a local basis size of $r = 12$. The corresponding single global ROM constructed from the same library achieves $E_{\text{global}} = 0.53$ with $r_{\text{global}} = 12$. Increasing the global ROM dimension decreases the relative error as shown in Figure 3, indicating that the global ROM requires a larger basis to reach comparable accuracy. Indeed, a basis size of $r_{\text{global}} = 21$ is required to obtain a comparable error of $E_{\text{global}} = 0.0078$. Overall, the results show that, for this trajectory, the local ROM method attains sufficient accuracy with substantially smaller local ROM dimension than the single global ROM.
Figure 1 also shows that the switching instances (denoted by vertical lines) cluster at early times. Since the trajectory is linear in $k$, it moves rapidly through the low-stiffness decades and progresses more slowly at high stiffness; consequently, the nearest neighbour selection $i(n)$ crosses multiple ROM boundaries in quick succession early on, while switches become increasingly sparse as $k(t)$ grows.

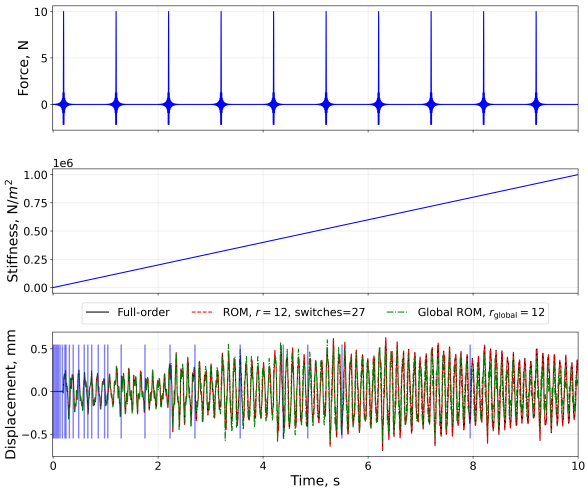


**Figure 1:** Comparison of the plate displacement at $(a/2, b/2)$ between the FOM, local ROMs, and single global ROM for a stiffness trajectory with a linear ramp over $[10^2, 10^6]$ N/m$^2$. The vertical blue lines indicate the time instance at which there is a switch in the local ROM.

We also assess a discontinuous stiffness trajectory defined by a Heaviside step, in which the boundary stiffness jumps from 200 N/m$^2$ to $7 \times 10^5$ N/m$^2$, as shown in Figure 2. For this case, the local ROM yields an error of $E_{\text{local}} = 0.016$ with a basis size of $r = 12$, while the global ROM yields a much larger relative error of $E_{\text{global}} = 0.98$ using the same ROM dimension.

Increasing the global ROM dimension decreases the relative error, as illustrated in Figure 3.

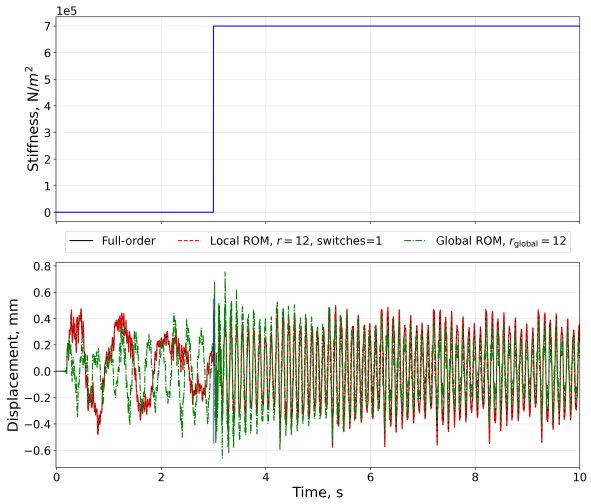


**Figure 2:** Comparison of the plate displacement at $(a/2, b/2)$ between the FOM, local ROMs, and single global ROM for a stiffness trajectory of a step from 200 N/m$^2$ to $7 \times 10^5$ N/m$^2$. The vertical blue lines indicate the time instance at which there is a switch in the local ROM.

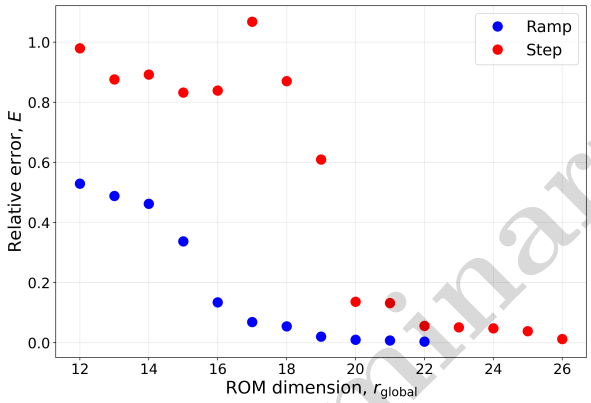


**Figure 3:** Effect of increasing the global ROM size on the relative error for two stiffness trajectories: (i) a Heaviside step from 200 N/m$^2$ to $7 \times 10^5$ N/m$^2$, and (ii) a linear ramp over $[10^2, 10^6]$ N/m$^2$.

## 6. Conclusion

This paper investigated a library-based POD-Galerkin ROM approach for second-order structural dynamics with time-varying boundary stiffness, using a Kirchhoff-Love plate supported by an edge spring. Local ROMs were trained offline at selected constant stiffness values using a ROM-ROM disagreement procedure. In the online phase, the time-varying response was predicted by selecting the appropriate (nearest) local ROM and transferring the reduced state between the reduced subspaces using a mass-orthogonal projection.

Numerical results demonstrate that the local reduced-order modelling approach can accurately reproduce the full-order response for stiffness trajectories within the training interval. A single global ROM was taken as a baseline comparison, which was constructed by performing a POD on the concatenated local bases used to form the library of local ROMs. In the case detailed in this paper, it was shown that a much larger global ROM dimension is required to achieve similar accuracy to the local reduced-order modelling approach.

It should be acknowledged that the proposed local reduced-order modelling approach incurs additional offline computations and storage costs compared with a single global ROM. These include the construction of multiple local POD bases, the coordinate alignment/basis rotations, and the state transfer computations. Moreover, the proposed approach assumes that the time-varying parameter $k(t)$ is available online to enable local ROM selection. However, in applications where $k(t)$ is not measured or uncertain, a single global ROM remains attractive due to the absence of parameter-dependent switching logic.

Future work will focus on extending the proposed local reduced-order modelling approach beyond the presented single-parameter plate by incorporating systems with multiple time-varying parameters. This will likely require ROM libraries whose structure scales efficiently with increasing parameter dimensionality.

## References


[1] M. Rathinam and L. R. Petzold, "A New Look at Proper Orthogonal Decomposition," *SIAM Journal on Numerical Analysis*, vol. 41, no. 5, pp. 1893–1925, Jan. 2003.

[2] P. Benner, S. Gugercin, and K. Willcox, "A Survey of Projection-Based Model Reduction Methods for Parametric Dynamical Systems," *SIAM Review*, vol. 57, no. 4, pp. 483–531, Jan. 2015.

[3] K. Kunisch and S. Volkwein, "Optimal snapshot location for computing POD basis functions," *ESAIM: Mathematical Modelling and Numerical Analysis*, vol. 44, no. 3, pp. 509–529, May 1, 2010.

[4] D. Amsallem, M. J. Zahr, and C. Farhat, "Nonlinear model order reduction based on local reduced-order bases," *International Journal for Numerical Methods in Engineering*, vol. 92, no. 10, pp. 891–916, 2012.

[5] J. Chung and G. M. Hulbert, "A Time Integration Algorithm for Structural Dynamics With Improved Numerical Dissipation: The Generalized-alpha Method," *Journal of Applied Mechanics*, vol. 60, no. 2, pp. 371–375, Jun. 1, 1993.

[6] J. C. Gower and G. B. Dijksterhuis, "Orthogonal Procrustes problems," in *Procrustes Problems*, J. C. Gower and G. B. Dijksterhuis, Eds., Oxford University Press, Jan. 22, 2004, pp. 29–47.